Wideband Polarization Insensitive Tunable Graphene-Supported Terahertz Metamaterial Absorber

Muhammad Abdul Jabbar, Muhammad Ashar Naveed, Muhammad Zubair, *Senior Member, IEEE*, Muhammad Qasim Mehmood, *Senior Member, IEEE*, and Yehia Massoud, *Fellow, IEEE*

***Abstract*—Broadband Terahertz (THz) metamaterial absorbers with tunable absorption characteristics have been attracting a lot of attention due to their high demand and utilization in advanced optical systems. Therefore, we propose a single-layer graphene-supported metamaterial absorber with a combination of square, circular and cross-shaped meta-resonators, exhibiting an outstanding absorption of more than 90% from 2.3 THz to 6.4 THz. The overall size of the unit cell is 15 $\times$ 15 μm^2, which holds graphene-based meta-resonators etched over a lossy dielectric substrate, backed by a 0.2 μm thick gold as a perfect reflector. This design architecture achieves the ultra-broadband absorption features by continuous design evaluation and optimization. The graphene-based metamaterial absorber (GMMA) reveals a polarization-insensitive response, and it also provides above 70% absorption for obliquely incident angles over the large operating bandwidth (2.3–6.4 THz). The polarization conversion ratio (PCR) also approached zero over the wideband of 4.1 THz and its maximum value of 16% was recorded at 4 THz. Furthermore, the amplitude spectra of the proposed GMMA is modulated from 19% to above 90% by stimulating the chemical potential of graphene from 0 eV to 0.7 eV. The simplified design configuration, broadband absorption features, and tunable capability of the GMMA provide the pathway to develop high-speed optical switches, THz detectors, and other opto-electronic devices.**

***Index Terms*—Absorber, broadband, graphene, PCR, terahertz, tunable.**

I. Introduction

THZ spectrum ranging from 0.1 to 10 THz received much attention due to their fascinating applications, including optical imaging, sensing, EM detection, THz switching, and 6G wireless communication systems [1], [2], [3], [4], [5], [6]. The THz band is less explored among the scientific community due to the paucity of naturally available materials in this band. Artificially engineered materials, which are also referred to as metamaterials, have gained much recognition from the research community owing to their intriguing and unusual features, such as Electromagnetic (EM) cloaking [7], optical lensing [8], holography [9], [10], [11], analog computing [12], bio-sensing [13], wireless communication [14], [15], and plasmon-induced transparency [16], etc. These are designed from periodic subwavelength-sized meta-resonators, holding various shapes, orientations, and geometries [17], [18], [19]. The manipulation of EM waves can be controlled through these artificially fashioned meta-molecules or meta-resonators, and many microwave and optical devices have been developed [20]. Moreover, metamaterials are exploited to implement a series of devices, namely optical filters, antennas, polarization rotators, beam-splitters, and EM absorbers [21], [22], [23], etc. Among all of these, perfect absorbers have been immensely employed in antenna isolation enhancement [24], stealth technology [25], radar cross-section reduction (RCSR) [26], thermophotovoltaics [27], and other optical communication systems [28], [29].

First of all, Landy et al. experimentally proved a near-unity metamaterial absorber (MMA) in 2008 [30]. Although this concept was proposed for the microwave frequency regime, thereafter, the deployment of meta-absorbers has been extended to the entire electromagnetic spectrum, ranging from microwave-ultraviolet [31], [32], [33]. As a result of this breakthrough, meta-absorbers have gained plenty of recognition due to their sub-wavelength thickness, low weight, high-efficiency, and spotless integration with microwave and optical devices. In literature, comprehensive studies were reported on narrow-band, wideband, polarization sensitive, and polarization-insensitive metamaterial absorbers for different frequency bands [34]. Further, dual band and multiband absorbers have importance especially in color filtering and absorption based sensing. However, dual band and multiband absorption can be achieved by employing multi resonance structures in single unit of absorber or more than one layers of structures [35], [36], [37], [38]. Consequently, while single narrow-band absorbers find prominent use in bio-optical sensing and filtering applications [39], [40], broadband absorbers have a broad spectrum of applications, including energy harvesting, electromagnetic shielding, bolometers, stealth technology, and numerous other fields [25], [26], [27], [28], [29].

Manuscript received 24 July 2023; revised 13 October 2023; accepted 17 October 2023. Date of publication 25 October 2023; date of current version 9 November 2023. This work was supported by the Innovative Technologies Laboratories (ITL) from King Abdullah University of Science and Technology (KAUST), Saudi Arabia. *(Muhammad Abdul Jabbar and Muhammad Ashar Naveed contributed equally to this work.) (Corresponding authors: Yehia Massoud; Muhammad Qasim Mehmood; Muhammad Zubair.)*

Muhammad Abdul Jabbar, Muhammad Ashar Naveed, and Yehia Massoud are with Innovative Technologies Laboratories (ITL), King Abdullah University of Science and Technology (KAUST), Thuwal 23955, Saudi Arabia (e-mail: msee17040@itu.edu.pk; ashargill106@gmail.com; yehia.massoud@kaust.edu.sa).

Muhammad Zubair and Muhammad Qasim Mehmood are with Micro-Nano Lab, Electrical Engineering Department, Information Technology University (ITU) of the Punjab, Lahore 54600, Pakistan (e-mail: muhammad.zubair3@kaust.edu.sa; qasim.mehmood@itu.edu.pk).

Digital Object Identifier 10.1109/JPHOT.2023.3327124

Usually, the basic design architecture of the metamaterial absorbers is composed of three layers (metal-dielectric-metal), where upper and lower layers are made of metal, and a dielectric spacer is placed between them. Besides, various design topologies, including multi-sized meta-resonators [41], multiple stacked-layers [23], and fractal-based meta-structures [42], are employed to attain the high absorption bandwidth of these metamaterial-based absorbers. Although the stacked-layers design scheme significantly enhances the absorption window, the practical implementation of this method is suffered due to the complex fabrication process and high cost, etc. On the other hand, fractal based design architectures are very difficult to fabricate because they consist of complex repeated structures organized in a specific pattern. On the contrary, multi-sized meta-structures based approach is far better than the stacked-layers and fractal. In this method, multi-sized meta-resonators are used to induce the multiple plasmonic resonances at different operating points and these resonances are merged to achieve the large absorption spectra. Thus, several THz broadband metamaterial based absorbers have been explored by using these aforesaid bandwidth-enhancing methods. The absorption spectra of these absorbers are fixed; however, we want post-fabrication control on spectral features (amplitude and frequency) so that the desired tunability and reconfigurability should be induced. Additionally, current and advanced communication systems demand miniaturized, broadband, and tunable metamaterial-based devices; therefore, there is a dire need to implement these meta-devices to fulfill the requirements of modern systems.

Graphene is a two-dimensional monolayer (atomic thickness) material that can change the optical characteristics of metamaterial-based devices by controlling the chemical potential of this material [43]. Graphene was discovered by Andre Geim and Konstantin Novoselov in 2004 [44], and it emerged as an alternative for developing ultrathin, highly efficient, and tunable optical devices. After this breakthrough, many researchers investigated graphene-based tunable and wideband absorbers for the THz band [45], [46]. For example, Fardoost et al. reported a terahertz metamaterial absorber with a wide absorption window of 2.7 THz [43], [44], [45], [46], [47]. The proposed absorber was composed of a multi-layer stacked configuration with three graphene and four dielectric layers. Besides, another investigation on graphene-supported multi-layer ultra-broadband THz absorber was reported in [44], [45], [46], [47], [48], which demonstrated a large absorption window of 4.8 THz. Similarly, Huang et al. investigated another multi-layer-based THz absorber, which showed a more than 90% absorption rate with a high absorption bandwidth of 2.68 THz [45], [46], [47], [48], [49]. A bi-layer graphene-based wideband THz absorber was also explored in [46], [47], [48], [49], [50], which presented an absorptivity of greater than 90% across an operating frequency from 2.54 THz to 3.70 THz. In addition, a wideband THz absorber is presented in [41], which possesses a single-layer device configuration with different multi-sized graphene-based meta-resonators grown over a SiO_2 dielectric substrate backed by the perfect mirror of gold. Furthermore, plenty of single-layer graphene-assisted THz metamaterial-based absorbers were also studied, which were composed of different design architectures, including concentric ring-cross [34], concentric double circular-rings [51] and concentric circular-ring with disk [52], etc. All of these, showed good absorption bandwidth, but the multi-layer design topology makes the fabrication process difficult and costly, hindering their practical implementation in integrated optical systems. Moreover, the single-layer design configuration also showed wideband absorption bandwidth, which can be further enhanced by carefully selecting the meta-structures and optimizing their design parameters.

In this study, authors investigate the ultra-broadband THz absorber, which comprises a cross-shaped meta-resonator surrounded by circular and square splitted meta-rings made of graphene. The proposed GMMA holds a single-layer device topology (metal-dielectric-metal), which possesses a top graphene metasurface placed over a gold-backed lossy dielectric substrate. The GMMA exhibits outstanding absorption results across a large THz band ranging from 2.3 to 6.4 THz, maintaining its absorption features under the effect of different oblique incident angles for both the transverse electric (TE) and transverse magnetic (TM) waves' excitation. To confirm the polarization-insensitivity of the GMMA, absorption spectra are also explored for various polarization angles of the THz waves. Furthermore, the absorption spectra switches from 19% to 90% by stimulating the chemical potential from 0 eV to 0.7 eV. The main contribution and novelty of the present work are as follows:

1) highest bandwidth for single-layer graphene metamaterial absorber with a small unit cell size ($15 \times 15\ \mu m^2$) according to the author's knowledge.
2) Smallest footprint of the meta-atom compared to the other single-layer metamaterial absorbers in the literature.
3) Simple and easily-fabricable geometry compared to the graphene-based multi-layer absorbers.
4) The above-mentioned features are attained without compromising the key attributes such as large absorption bandwidth, amplitude-tunability, polarization insensitivity, and wide angular stability.

II. Design and Simulation

The GMMA design consists of a cross-shaped meta-structure surrounded with circular and square meta-rings, which are placed on the top of the TOPAS substrate, backed with a gold layer having a conductivity of 4.5×10^7 S/m. The dielectric constant and thickness of substrate are 2.35 and 11 μm, respectively. The two-dimensional (2D) and three-dimensional (3D) views of the GMMA are shown in Figs. 1(a) and (b) and (c) explicates the 3D periodic arrays of the graphene-based meta-resonators. There is a 0.2 μm gold layer under the substrate to completely block the transmission of electromagnetic THz waves. By using the Drude model the conductivity of the gold was calculated which is $\sigma = 4.56 \times 10^7$ S/m. The periodicity (P) of the proposed GMMA is selected as 15 μm with a square ring of the same length but different width of 2 μm. The circular ring's outer radius (r) is chosen to be 5.2 μm with a ring width (w_3) of 1.70 μm. Furthermore, the length (l_2) and width (w_2) of the inner cross-shaped meta-ring have been optimized, and they are selected as 6 μm and 0.85 μm, respectively. In addition, the

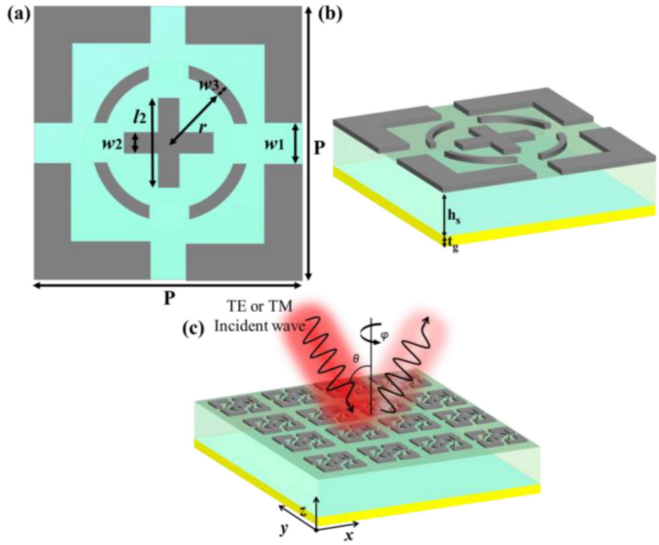

Fig. 1. Representation of schematic diagram of the proposed GMMA, (a) top view of the designed unit cell of the proposed GMMA, (b) 3-D view of the unit cell of the proposed GMMA, and (c) 3D view of periodic arrays of the meta-resonators of the proposed GMMA.

parameter w_1 which denotes the length of splits in circular and square rings, is chosen as 1.73 μm.

Graphene with an ultra-thin atomic layer is considered a 2D material, and its surface conductivity $\sigma(\omega)$ can be described using Kubo's equation as shown in the following equations [29]:

$$\boldsymbol{\sigma}\ (\boldsymbol{\omega}, \boldsymbol{\mu_c}, \boldsymbol{\Gamma}, \mathbf{T}) = \boldsymbol{\sigma_{intra}} + \boldsymbol{\sigma_{inter}}, \tag{1}$$

$$\boldsymbol{\sigma_{intra}} = \frac{\boldsymbol{je^2}}{\boldsymbol{\pi\hbar^2}\,(\boldsymbol{\omega} - \mathbf{j2\Gamma})} \times \int_0^{\infty} \boldsymbol{\xi}\left(\frac{\partial \boldsymbol{f_d}\,(\boldsymbol{\omega}, \boldsymbol{\mu_c}, \mathbf{T})}{\partial \boldsymbol{\xi}} - \frac{\partial \boldsymbol{f_d}\,(-\boldsymbol{\xi}, \boldsymbol{\mu_c},\ \mathbf{T})}{\partial \boldsymbol{\xi}}\right) \boldsymbol{d_\xi}, \tag{2}$$

$$\boldsymbol{\sigma_{intra}} = \frac{\boldsymbol{je^2}\,(\boldsymbol{\omega} - \boldsymbol{j2\Gamma})}{\boldsymbol{\pi\hbar^2}} \int_0^{\infty} \frac{\boldsymbol{f_d}\,(-\boldsymbol{\xi}, \boldsymbol{\mu_c},\ \mathbf{T}) - \boldsymbol{f_d}\,(\boldsymbol{\xi}, \boldsymbol{\mu_c},\ \mathbf{T})}{(\boldsymbol{\omega} - \boldsymbol{j2\Gamma})^2\ -\ 4(\frac{\boldsymbol{\xi}}{\hbar})^2} \boldsymbol{d_\xi}, \tag{3}$$

$$\boldsymbol{f_d}\ (\boldsymbol{\xi}, \boldsymbol{\mu_c}, \mathbf{T}) = \left(\boldsymbol{e}^{\frac{(\boldsymbol{\xi} - \boldsymbol{\mu_c})}{\boldsymbol{K_B T}}} + 1\right)^{-1}. \tag{4}$$

In the above equations, σ_{intra} and σ_{inter} are derived from intra- and inter-band transitions. However, $f_d\,(\xi,\mu_c,T)$ is Fermi-Dirac distribution, radiation frequency ω, electron charge e, Boltzmann constant is K_B, T is the temperature in Kelvin, $\bar{h}$ reduced Plank Constant, Scattering rate $\Gamma = (1/2\tau)$, τ is electron-photon relaxation time, ξ is electron energy, and μ_c is chemical potential. At 300 K room temperature, the intra-band transition is more dominant than the inter-band transition. So, we can write the above Kubo equation in a reduced Durde–like equation, as given below [34].

$$\boldsymbol{\sigma}\ = \frac{\boldsymbol{je^2\mu_c}}{\boldsymbol{\pi\hbar^2}\,(\boldsymbol{\omega} + \boldsymbol{j\tau^{-1}})}. \tag{5}$$

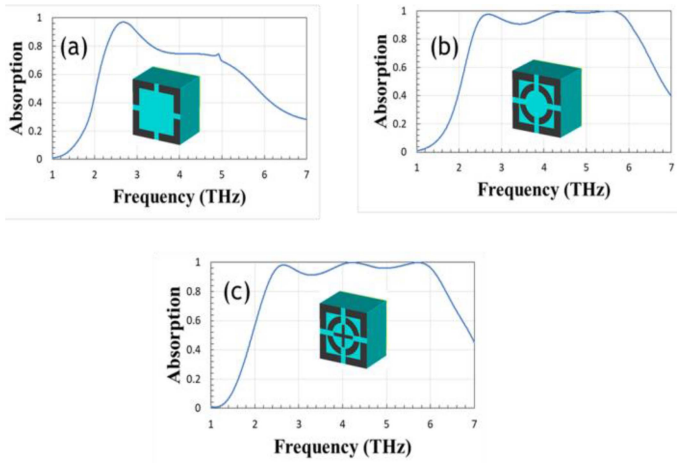

Fig. 2. Design evaluation and optimization along with the absorption of the proposed GMMA. (a) A simple square-splitted graphene meta-ring, (b) a combination of the square-circular-splitted graphene meta-rings, and (c) a combination of the square-circular-splitted and cross-shaped meta-resonators.

According to (5), surface conductivity depends on three parameters, such as τ, μ_c, and ω. Initially, the values of the τ and μ_c set to the highest value of 1 for simulation purposes.

Furthermore, to explore the results of the GMMA, we set the boundary conditions as the unit cell in both directions along the x and y-axis, whereas setting the open add space along the z-axis. When an EM THz wave strikes the absorber from above, impedance matching between the free space and the absorber causes the EM wave to penetrate the entire structure of the meta-absorber. The incident EM wave get trapped in the dielectric substrate and absorption A(λ) can be represented as $A(\omega) = 1 - R(\omega) - T(\omega)$, where $A(\omega)$, $R(\omega)$ and $T(\omega)$ represent the total absorption, reflection, and transmission of the proposed absorber. The above given reflection and transmission parameters can be written in form of scattering, such as $A(\omega) = 1 - |S_{11}\,(\omega)|^2 - |S_{21}\,(\omega)|^2$. However, the metal layer under the substrate act as a reflector, and overall transmission $T(\omega)$ result in zero. The reflection coefficient can also be represented in terms of the s-parameters so that the total absorption can be written as $A(\omega) = 1 - |S_{11}|^2$.

III. Results and Discussion

This section evaluates each design stage's absorption features by exposing the metamaterial under the normally incident THz radiation. To achieve wideband absorption, we initially placed a square split-ring on the top of the substrate, as shown in Fig. 2(a). In this case, a plasmonic resonance is induced around 2.65 THz, and the absorption is above 90% for a small frequency band from 2.6 to 3 THz. Furthermore, a circular split-ring is added inside the square split-ring, as shown in Fig. 2(b). As a result, another plasmonic resonance is noticed at 4.2 THz, and a broad absorption spectrum is obtained ranging from 2.6–6 THz. The enhanced absorption bandwidth is attributed to combining two plasmonic resonances generated by square and circular split-ring. In addition, another cross-shaped meta-resonator is incorporated inside the circular split-ring to further increase the

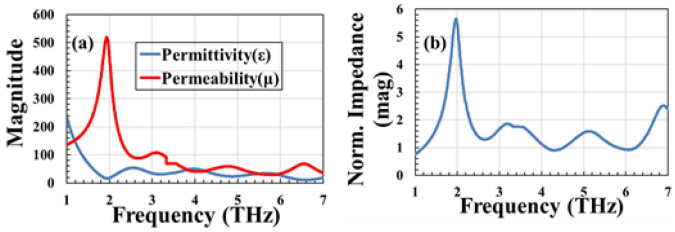

Fig. 3. Optical parameters of the proposed GMMA, (a) magnitude of permittivity and permeability of the proposed GMMA, and (b) magnitude of the normalized impedance of the proposed GMMA.

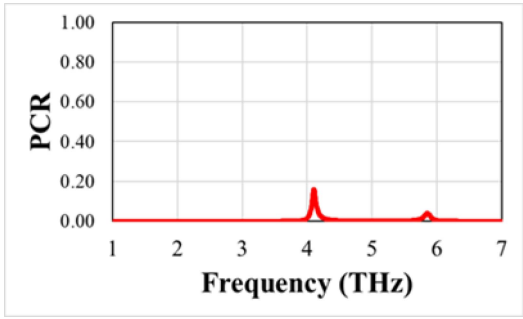

Fig. 4. Outcome of polarization conversion Ratio (PCR) for proposed meta-absorber.

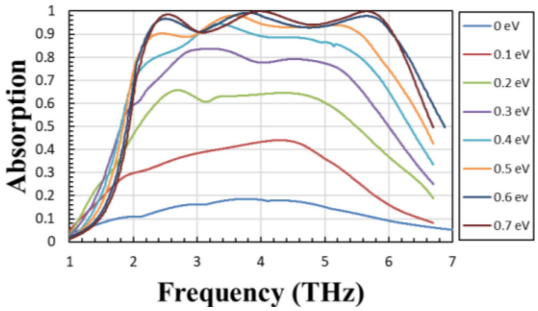

Fig. 5. Amplitude modulation of the proposed GMMA under the stimulation of the chemical potential of the graphene.

absorption window of the proposed GMMA. It is obvious in Fig. 2(c) that the absorption spectra of the designed GMMA were significantly enhanced after the inclusion of a cross-shaped meta-resonator, and it illustrates a high absorption bandwidth from 2.3 THz to 6.4 THz. Compared to all three stages, the final stage performs well and shows outstanding absorption features with an overall bandwidth of 4.1 THz.

In case of GMMA, the impedance matching $Z_{\text{meta}} = \sqrt{\mu_{\text{meta}}/\varepsilon_{\text{meta}}}$ plays a vital role. Here, μ_{meta} and $\varepsilon_{\text{meta}}$ represent the permeability and permittivity of the designed GMMA. Perfect impedance matching is a necessary condition for high absorption; the impedance of GMMA must be equal to free space ($Z_o = 377\Omega$) impedance. Equation 6 aids in calculating the normalized effective impedance [19].

$$\boldsymbol{Z_{eff}} = \sqrt{\frac{(1+\boldsymbol{S}_{11})^2 - \boldsymbol{S}_{21}^2}{(1-\boldsymbol{S}_{11})^2 - \boldsymbol{S}_{21}^2}} = \frac{1+\boldsymbol{S}_{11}}{1-\boldsymbol{S}_{11}}. \tag{6}$$

When it goes to 0, then absorption approach to maximum value means 100%. As the transmission is zero already due to the usage of perfect conducting Gold layer. Therefore, the idea of permittivity and permeability is crucial to the absorption characteristics and validation of the proposed GMMA. The normalised impedance should be one when both of these parameters have equal magnitudes under ideal absorption conditions. Fig. 3(a) represents the magnitude of permittivity and permeability, respectively. The effective impedance should be unity at perfect matching operating points, such as $Z/Z_0 = \sqrt{\mu_o/\varepsilon_o} = 1$ [53].

According to Fig. 3(a), these parameters overlap all the way from 2.3 to 6.4 THz. As previously stated, the GMMA offers above 90% absorption throughout this whole bandwidth. Thus, the effective impedance lies between 1 and 2, as depicted in Fig. 3(b) showing the perfect impedance matching condition. To gain a in-depth understanding of the meta-absorber, polarization conversion plays a pivotal role. Therefore, we analyze the Polarization Conversion Ratio (PCR) within the specific frequency range of interest. The calculation of PCR implicates dividing the square of cross-polarized reflection $|r_{xy}|^2$ coefficient by the addition of the squares of the co-polarized $|r_{yy}|^2$ coefficient and cross-polarized $|r_{xy}|^2$ coefficient [54]. Here, (7) is used for the calculation of PCR, when an electromagnetic wave is linearly y-polarized.

$$\text{PCR} = \frac{|\boldsymbol{r_{xy}}|^2}{|\boldsymbol{r_{yy}}|^2 + |\boldsymbol{r_{xy}}|^2} \tag{7}$$

The PCR value is almost zero over the whole operating frequency band, as shown in Fig. 4. The maximum PCR of 16% occurs at 4 THz, which can be considered relatively very low.

Furthermore, another crucial performance parameter for contemporary metamaterial-based devices is their tunability. In this context, we assess the tunability of the suggested GMMA by modifying the chemical potential of graphene while keeping the relaxation time (t_s) constant at 0.1 ps. Fig. 5 depicts the amplitude-based tunability of the GMMA by changing the chemical potential of the graphene from 0 to 0.7 eV. The value of the absorption spectra increases as we change the chemical potential from 0 to 0.7 eV, and the proposed GMMA demonstrates more than 90% absorption rate with a bandwidth of 4.1 THz for $\mu_c = 0.7$ eV. This change in absorption features is similar to optical switching phenomena that can be designed by controlling the chemical potential of graphene. Therefore, such functionality could effectively implement high-speed optical switches and Boolean logic gates in advanced optical systems. Furthermore, graphene's relaxation time also significantly impacts the absorption behavior of the proposed GMMA; therefore, it varies from 0 to 0.6 ns, as depicted in Fig. 6. Conversely, absorption decreases by changing the relaxation time from 0.1 to 0.6 ps. The relaxation time of 0.6 ns is observed to exhibit the minimum 50% absorption throughout the entire frequency range (Fig. 6).

Moreover, surface electric field analysis is also performed at three plasmonic resonances, namely 2.65 THz, 4.2 THz, and 5.72 THz. The surface electric field distribution plays an intuitive role in the physical understanding of the absorption phenomena of the proposed GMMA, as shown in Fig. 7. The GMMA

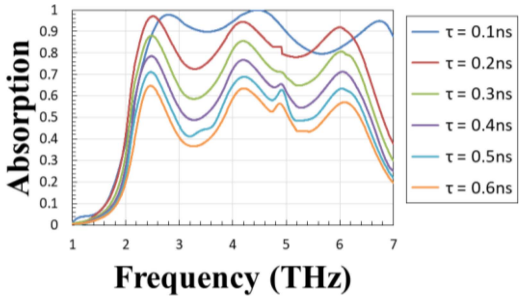

Fig. 6. Amplitude modulation of the proposed GMMA under the stimulation of relaxation time of the graphene.

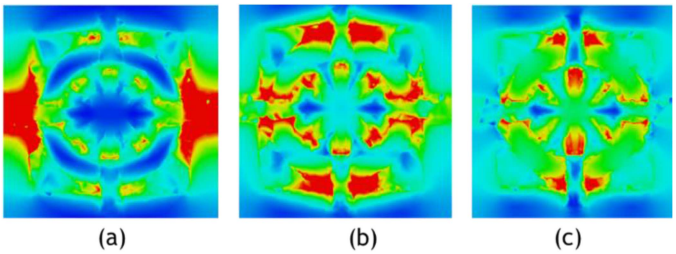

Fig. 7. Illustration of the surface electric field intensity of the proposed GMMA for three different plasmonic resonances (a) frequency point at 2.62 THz, (b) frequency point at 4.13 THz, and (c) frequency point at 5.82 THz.

produces a dipole-like surface electric field pattern along the horizontal edges of the outer square split-ring, which causes a maximum absorption peak at 2.65 THz. For the 4.2 THz case, both square and circular rings create dipole-like phenomena, and the maximum E-field is concentrated at the vertical edges of the square split-ring and horizontal edges of the circular split-ring; these two rings are the main contributor to creating the plasmonic resonance at 4.2 THz. Finally, at the higher frequency of 5.72 THz, E-field intensity is maximally accumulated at the two inner meta-resonators (circular & cross), and as a result, another plasmonic resonance is generated. These three plasmonic resonances collectively couple with each other, and a large absorption bandwidth is obtained.

Furthermore, the polarization sensitivity of the proposed GMMA is a key performance parameter, and it is also evaluated by varying the azimuthal angle (φ) from 0° to 90° with a step size of 15°. Here 0° and 90° represent the incident EM wave along the x- and y-axis, respectively. Fig. 8 reveals that the absorption remains unchanged by varying φ from 0° to 90°. Therefore, the absorption of the proposed GMMA is insensitive to the influence of polarization angles, and this functionality is attributed to the four-fold symmetric nature of the designed GMMA [55].

The functionality of metamaterial absorbers is also influenced by angular stability, so the GMMA's absorption characteristics are examined by varying the oblique incidence angle from 0° to 60° with increasing step widths of 10°. Fig. 9(a) and (b) show the absorption plot for TE and TM incident polarizations. In the case of TE polarization, the average absorption maintains a level of $\geq$ 90% for the oblique incident angle $\leq$ 30°. The absorption starts to decrease as the oblique angle increased from 30°, but it still

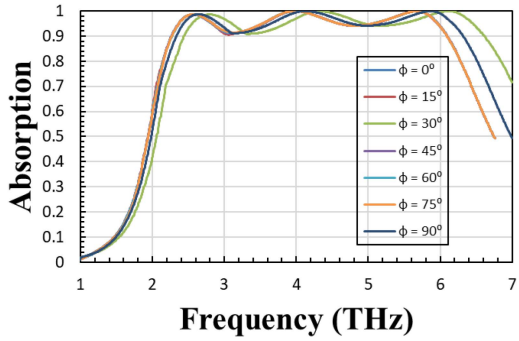

Fig. 8. Analysis of optical absorption characteristics of the proposed GMMA under the inspection of various polarization angles (φ).

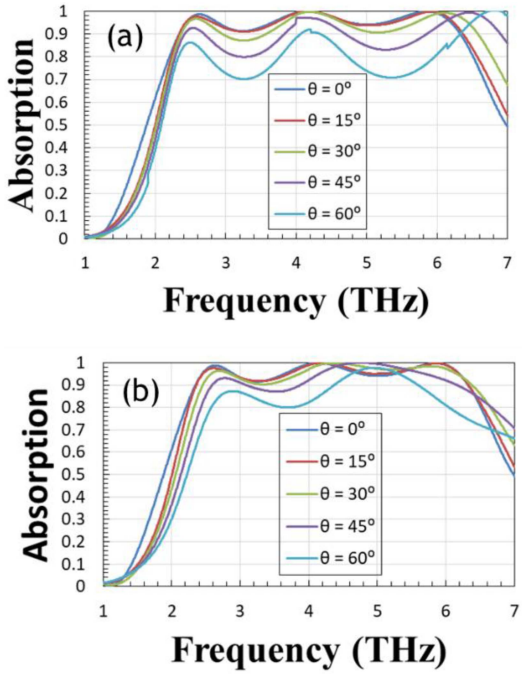

Fig. 9. Analysis of optical absorption characteristics of the proposed GMMA under the inspection of various oblique incident angles (θ), (a) TE-wave polarization case, and (b) TM-wave polarization case.

remains at more than 70% threshold until $\theta \leq 60°$. However, in the case of TM polarization, the entire absorption window maintains its value above $\geq$ 90% for $\theta \leq 45°$. Meanwhile, for $45° < \theta \leq 60°$, absorption decreases from 90% to 80%, and there is a sharp decrease at higher frequencies. Overall, the proposed GMMA exhibited a stable absorption performance under the influence of oblique incident angles.

Furthermore, to validate the advantages of the present GMMA, a comparative analysis is also performed in Table I. This table discusses the advantages and disadvantages of various graphene-based THz absorbers. According to the comparative analysis, the GMMA outperforms the most advanced graphene-based THz absorbers in terms of absorption performance. For example, the absorption bandwidth of all the THz absorbers is less than that of our proposed GMMA, except for

TABLE I
COMPARISON OF THE ABSORPTION FEATURES OF STATE-OF-THE-ART THZ GRAPHENE-BASED ABSORBERS WITH THE PRESENT STUDY

Design architecture	Constitutive materials	Device-layers	Bandwidth > 90 %	Size (μm²)	Angle stability absorption > 70 %
Concentric ring-cross resonators [34]	Graphene, TOPAS, and gold	Single	0.76 THz	73 × 73	θ = 60°
Octagon with annular strips [41]	Graphene, SiO_2, and gold	Single	0.93 THz	80 × 80	θ = 70°
Square fan-like patches [47]	Graphene, TOPAS, and gold	Multiple stacked	2.7 THz	15 × 15	Not given
Rectangular strips [48]	Graphene, SiO_2, TOPAS and gold	Multiple stacked	4.8 THz	32 × 32	θ = 70°
Square-pillars [49]	Graphene, polyimide, and gold	Multiple stacked	2.68 THz	118 × 118	θ = 60°
Windmill structure [50]	Graphene, SiO_2, and gold	Double	1.16 THz	71 × 71	θ = 60°
Concentric dual circular rings [51]	Graphene, SiO_2, and gold	Single	0.46 THz	15 × 15	θ = 60°
Concentric circular rings and disks [47]	Graphene, polymer, and gold	Single	1.57 THz	75 × 75	θ = 70°
Circular disks [56]	Graphene, SiO_2 and gold	Single	1.22 THz	35 × 35	θ = 60°
Hollow-out square with slender strips [57]	Graphene, TOPAS, and silver	Single	3.33 THz	69.5 × 69.5	θ = 70°
Square patches [58]	Graphene, TOPAS, and gold	Multiple stacked	2.66 THz	30 × 30	θ = 60°
Circlre, ring and arc [59]	Polyimide, Silicon and Copper	Single	0.98 THz	144 × 144	θ = 45°
Split ring resonator and L shape groves [60]	Copper, Mercury and FR4	Single	2.73 THz	169 × 169	θ = 60°
Direction dependent Janus metasurface supported by waveguide [61]	Gold and SiO2	Single	0.4 THz	150 × 150	NA
Graphene-embedded photonic crystals [62]	SiO_2, Graphene, Gold, and Synthetic Dielectric	Multiple	5.71 THz	NA	θ = 60°
Splitted squares and circular rings with crosses (This work)	Graphene, TOPAS, and gold	Single	4.1 THz	15 × 15	θ = 60°

the [43] having 4.8 THz; however, its geometry is comprised of multiple graphene and dielectric layers based on a stacked configuration. On the other hand, our proposed GMMA holds a single-layer-based device configuration with a small size of 15×15 μm^2. Furthermore, the proposed GMMA possesses simple and easily-fabricable geometry, while multi-layer-based design architectures restrict their practical implementation due to the complex fabrication process and high cost.

IV. CONCLUSION

In this paper, we proposed an ultra-wideband metamaterial absorber with a combination of square, circular, and cross-shaped resonators that is tunable and polarization-insensitive for THz applications. The numerical absorption approaches above 90% over the entire THz frequencies from 2.3 to 6.4 THz. Furthermore, the inclusion of inner circular and cross-shaped resonators increase the overall bandwidth by enabling the phenomena of mutual coupling resonance. The polarization conversion ratio (PCR) also approached zero over the wideband of 4.1 THz and its maximum value of 16% was recorded at 4 THz. The amplitude-based tunable characteristics of GMMA are evaluated by varying graphene's chemical potential and relaxation time from 0 to 0.7 eV and 0.1 to 0.6 ps, respectively. Under the variation of chemical potential, the GMMA absorption increased from 19% to above 90% while absorption decreased to 35% as relaxation time approached to 0.6 ps over the entire bandwidth of 4.1 THz. In addition, the GMMA achieved above 70% absorption for both TE and TM polarization at oblique incident angles. Thus, simple design architecture and outstanding performance make this GMMA a promising alternative for developing high-speed optical switches and intelligent absorbers.

REFERENCES

[1] D. Mittleman, M. Gupta, R. Neelamani, R. Baraniuk, J. Rudd, and M. Koch, "Recent advances in terahertz imaging," *Appl. Phys. B*, vol. 68, pp. 1085–1094, 1999.
[2] C. Debus and P. H. Bolivar, "Frequency selective surfaces for high sensitivity terahertz sensing," *Appl. Phys. Lett.*, vol. 91, no. 18, 2007, Art. no. 184102.
[3] M. Zhang and Z. Song, "Switchable terahertz metamaterial absorber with broadband absorption and multiband absorption," *Opt. Exp.*, vol. 29, no. 14, pp. 21551–21561, 2021.
[4] Z. Zhou and Z. Song, "Terahertz mode switching of spin reflection and vortex beams based on graphene metasurfaces," *Opt. Laser Technol.*, vol. 153, 2022, Art. no. 108278.
[5] B. Chen et al., "Directional terahertz holography with thermally active Janus metasurface," *Light: Sci. Appl.*, vol. 12, no. 1, 2023, Art. no. 136.

[6] X. K. Wang, J. S. Ye, W. F. Sun, P. Han, L. Hou, and Y. Zhang, "Terahertz near-field microscopy based on an air-plasma dynamic aperture," *Light: Sci. Appl.*, vol. 11, no. 1, 2022, Art. no. 129.

[7] D. Schurig et al., "Metamaterial electromagnetic cloak at microwave frequencies," *Science*, vol. 314, no. 5801, pp. 977–980, 2006.

[8] N. Mahmood et al., "Ultraviolet–Visible multifunctional vortex metaplates by breaking conventional rotational symmetry," *Nano Lett.*, vol. 23, pp. 1195–1201, 2023.

[9] M. A. Naveed et al., "Optical spin-symmetry breaking for high-efficiency directional helicity-multiplexed metaholograms," *Microsystems Nanoeng.*, vol. 7, no. 1, 2021, Art. no. 5.

[10] M. Q. Mehmood et al., "Single-cell-driven tri-channel encryption metadisplays," *Adv. Sci.*, vol. 9, no. 35, 2022, Art. no. 2203962.

[11] A. J. Satti et al., "A highly efficient broadband multi-functional metaplate," *Nanoscale Adv.*, vol. 5, no. 7, pp. 2010–2016, 2023.

[12] F. Zangeneh-Nejad, D. L. Sounas, A. Alù, and R. Fleury, "Analogue computing with metamaterials," *Nature Rev. Mater.*, vol. 6, no. 3, pp. 207–225, 2021.

[13] H. Altug, S.-H. Oh, S. A. Maier, and J. Homola, "Advances and applications of nanophotonic biosensors," *Nature Nanotechnol.*, vol. 17, no. 1, pp. 5–16, 2022.

[14] Q. Ma et al., "Directly wireless communication of human minds via non-invasive brain-computer-metasurface platform," *eLight*, vol. 2, no. 1, pp. 1–11, 2022.

[15] R. Zhu et al., "Remotely mind-controlled metasurface via brainwaves," *eLight*, vol. 2, no. 1, pp. 1–11, 2022.

[16] R. M. H. Bilal, M. A. Baqir, P. K. Choudhury, M. M. Ali, and A. A. Rahim, "Tunable and multiple plasmon-induced transparency in a metasurface comprised of silver S-shaped resonator and rectangular strip," *IEEE Photon. J.*, vol. 12, no. 3, Jun. 2020, Art. no. 4500913.

[17] M. A. Naveed et al., "Novel spin-decoupling strategy in liquid crystal-integrated metasurfaces for interactive metadisplays," *Adv. Opt. Mater.*, vol. 10, no. 13, 2022, Art. no. 2200196.

[18] B. Xiong, L. Deng, R. Peng, and Y. Liu, "Controlling the degrees of freedom in metasurface designs for multi-functional optical devices," *Nanoscale Adv.*, vol. 1, no. 10, pp. 3786–3806, 2019.

[19] I. Javed et al., "Broad-band polarization-insensitive metasurface holography with a single-phase map," *ACS Appl. Mater. Interfaces*, vol. 14, no. 31, pp. 36019–36026, 2022.

[20] K. Iqbal and Q. U. Khan, "Review of metasurfaces through unit cell design and numerical extraction of parameters and their applications in Antennas," *IEEE Access*, vol. 10, pp. 112368–112391, 2022.

[21] J. Wang et al., "Metantenna: When metasurface meets antenna again," *IEEE Trans. Antennas Propag.*, vol. 68, no. 3, pp. 1332–1347, Mar. 2020.

[22] T. Ahmad et al., "Ultrawideband cross-polarization converter using anisotropic reflective metasurface," *Electronics*, vol. 11, no. 3, 2022, Art. no. 487.

[23] S. Mehrabi, R. M. H. Bilal, M. A. Naveed, and M. M. Ali, "Ultra-broadband nanostructured metamaterial absorber based on stacked square-layers of TiN/TiO 2," *Opt. Mater. Exp.*, vol. 12, no. 6, pp. 2199–2211, 2022.

[24] P. Garg and P. Jain, "Isolation improvement of MIMO antenna using a novel flower shaped metamaterial absorber at 5.5 GHz WiMAX band," *IEEE Trans. Circuits Syst. II: Exp. Briefs*, vol. 67, no. 4, pp. 675–679, Apr. 2020.

[25] K. Iwaszczuk, A. C. Strikwerda, K. Fan, X. Zhang, R. D. Averitt, and P. U. Jepsen, "Flexible metamaterial absorbers for stealth applications at terahertz frequencies," *Opt. Exp.*, vol. 20, no. 1, pp. 635–643, 2012.

[26] S. Sui et al., "Absorptive coding metasurface for further radar cross section reduction," *J. Phys. D: Appl. Phys.*, vol. 51, no. 6, 2018, Art. no. 065603.

[27] A. Shafique, M. A. Naveed, S. Ijaz, M. Zubair, M. Q. Mehmood, and Y. Massoud, "Highly efficient Vanadium nitride based metasurface absorber/emitter for solar-thermophotovoltaic system," *Mater. Today Commun.*, vol. 34, 2023, Art. no. 105416.

[28] Y. Zhang, H. Dong, N. Mou, L. Chen, R. Li, and L. Zhang, "High-performance broadband electromagnetic interference shielding optical window based on a metamaterial absorber," *Opt. Exp.*, vol. 28, no. 18, pp. 26836–26849, 2020.

[29] Y. Zhou et al., "Ultra-broadband metamaterial absorbers from long to very long infrared regime," *Light: Sci. Appl.*, vol. 10, no. 1, 2021, Art. no. 138.

[30] N. I. Landy, S. Sajuyigbe, J. J. Mock, D. R. Smith, and W. J. Padilla, "Perfect metamaterial absorber," *Phys. Rev. Lett.*, vol. 100, no. 20, 2008, Art. no. 207402.

[31] R. Bilal et al., "Elliptical metallic rings-shaped fractal metamaterial absorber in the visible regime," *Sci. Rep.*, vol. 10, no. 1, 2020, Art. no. 14035.

[32] M. A. Naveed, R. M. H. Bilal, A. A. Rahim, M. A. Baqir, and M. M. Ali, "Polarization-insensitive dual-wideband fractal meta-absorber for terahertz applications," *Appl. Opt.*, vol. 60, no. 29, pp. 9160–9166, 2021.

[33] K. Liu et al., "Super absorbing ultraviolet metasurface," *IEEE Photon. Technol. Lett.*, vol. 27, no. 14, pp. 1539–1542, Jul. 2015.

[34] H. Feng et al., "Tunable polarization-independent and angle-insensitive broadband terahertz absorber with graphene metamaterials," *Opt. Exp.*, vol. 29, no. 5, pp. 7158–7167, 2021.

[35] A. Jabbar, M. A. Naveed, I. Javed, and Y. Massoud, "Chromium-nanostructured metabsorber for tunable color filtering," *Proc. SPIE*, vol. 12322, pp. 62–68, 2022.

[36] D. Yan, M. Meng, J. Li, and X. Li, "Graphene-assisted narrow bandwidth dual-band tunable terahertz metamaterial absorber," *Front. Phys.*, vol. 8, 2020, Art. no. 306.

[37] D. Wang, K.-D. Xu, S. Luo, Y. Cui, L. Zhang, and J. Cui, "A high Q-factor dual-band terahertz metamaterial absorber and its sensing characteristics," *Nanoscale*, vol. 15, no. 7, pp. 3398–3407, 2023.

[38] R. Gao, Z. Xu, C. Ding, L. Wu, and J. Yao, "Graphene metamaterial for multiband and broadband terahertz absorber," *Opt. Commun.*, vol. 356, pp. 400–404, 2015.

[39] Q. Xie, G. Dong, B.-X. Wang, and W.-Q. Huang, "Design of quad-band terahertz metamaterial absorber using a perforated rectangular resonator for sensing applications," *Nanoscale Res. Lett.*, vol. 13, no. 1, pp. 1–8, 2018.

[40] S. Song et al., "Tailoring active color rendering and multiband photodetection in a vanadium-dioxide-based metamaterial absorber," *Photon. Res.*, vol. 6, no. 6, pp. 492–497, 2018.

[41] H. Yu, P. Xiang, Y. Zhu, S. Huang, and X. Luo, "Polarization insensitive broadband concentric-annular-strip octagonal terahertz graphene metamaterial absorber," *IEEE Photon. J.*, vol. 14, no. 1, Feb. 2022, Art. no. 4600906.

[42] R. Bilal, M. Naveed, M. Baqir, M. Ali, and A. Rahim, "Design of a wideband terahertz metamaterial absorber based on pythagorean-tree fractal geometry," *Opt. Mater. Exp.*, vol. 10, no. 12, pp. 3007–3020, 2020.

[43] Y. Zhang, Y. Feng, B. Zhu, J. Zhao, and T. Jiang, "Graphene based tunable metamaterial absorber and polarization modulation in terahertz frequency," *Opt. Exp.*, vol. 22, no. 19, pp. 22743–22752, 2014.

[44] K. S. Novoselov et al., "Electric field effect in atomically thin carbon films," *Science*, vol. 306, no. 5696, pp. 666–669, 2004.

[45] H. Chen, W. Ma, Z. Huang, Y. Zhang, Y. Huang, and Y. Chen, "Graphene-based materials toward microwave and terahertz absorbing stealth technologies," *Adv. Opt. Mater.*, vol. 7, no. 8, 2019, Art. no. 1801318.

[46] S. Zakir et al., "Polarization-insensitive, broadband, and tunable terahertz absorber using slotted-square graphene meta-rings," *IEEE Photon. J.*, vol. 15, no. 1, Feb. 2023, Art. no. 4600108.

[47] A. Fardoost, F. Ghaedi Vanani, S. A. Amirhosseini, and R. Safian, "Design of multi-layer graphene based ultra wideband terahertz absorber," *IEEE Trans. Nanotechnol.*, vol. 16, no. 1, pp. 68–74, Jan. 2017, doi: 10.1109/tnano.2016.2627939.

[48] Z. Xu et al., "Design of a tunable ultra-broadband terahertz absorber based on multiple layers of graphene ribbons," *Nanoscale Res. Lett.*, vol. 13, no. 1, pp. 1–8, 2018.

[49] X. Huang, M. Cao, D. Wang, X. Li, J. Fan, and X. Li, "Broadband polarization-insensitive and oblique-incidence terahertz metamaterial absorber with multi-layered graphene," *Opt. Mater. Exp.*, vol. 12, no. 2, pp. 811–822, 2022.

[50] J. Xu et al., "Broadband tunable perfect absorber with high absorptivity based on double layer graphene," *Opt. Mater. Exp.*, vol. 11, no. 10, pp. 3398–3410, 2021.

[51] N. Mou et al., "Hybridization-induced broadband terahertz wave absorption with graphene metasurfaces," *Opt. Exp.*, vol. 26, no. 9, pp. 11728–11736, 2018.

[52] X. Huang, W. He, F. Yang, J. Ran, B. Gao, and W.-L. Zhang, "Polarization-independent and angle-insensitive broadband absorber with a target-patterned graphene layer in the terahertz regime," *Opt. Exp.*, vol. 26, no. 20, pp. 25558–25566, 2018.

[53] M. A. Naveed, R. M. H. Bilal, M. A. Baqir, M. M. Bashir, M. M. Ali, and A. A. Rahim, "Ultrawideband fractal metamaterial absorber made of nickel operating in the UV to IR spectrum," *Opt. Exp.*, vol. 29, no. 26, pp. 42911–42923, 2021.

[54] G. Deng, H. Sun, K. Lv, J. Yang, Z. Yin, and B. Chi, "An efficient wideband cross-polarization converter manufactured by stacking metal/dielectric multilayers via 3D printing," *J. Appl. Phys.*, vol. 127, no. 9, 2020, Art. no. 093103.

[55] R. M. H. Bilal, M. A. Saeed, M. A. Naveed, M. Zubair, M. Q. Mehmood, and Y. Massoud, "Nickel-based high-bandwidth nanostructured metamaterial absorber for visible and infrared spectrum," *Nanomaterials*, vol. 12, no. 19, 2022, Art. no. 3356.

[56] D. Hu, T. Meng, H. Wang, and Y. Ma, "Tunable broadband terahertz absorber based on plasmon hybridization in monolayer graphene ring arrays," *Appl. Opt.*, vol. 59, no. 35, pp. 11053–11058, 2020.

[57] J. Han and R. Chen, "Tunable broadband terahertz absorber based on a single-layer graphene metasurface," *Opt Exp.*, vol. 28, no. 20, pp. 30289–30298, Sep. 2020, doi: 10.1364/OE.403631.

[58] L. Liu, W. Liu, and Z. Song, "Ultra-broadband terahertz absorber based on a multilayer graphene metamaterial," *J. Appl. Phys.*, vol. 128, no. 9, 2020, Art. no. 093104.

[59] S. Liao, J. Sui, and H. Zhang, "Switchable ultra-broadband absorption and polarization conversion metastructure controlled by light," *Opt. Exp.*, vol. 30, no. 19, pp. 34172–34187, 2022.

[60] J. Qu, H. Pan, Y. Z. Sun, and H. F. Zhang, "Multitasking device regulated by the gravity field: Broadband anapole-excited absorber and linear polarization converter," *Annalen der Physik*, vol. 534, no. 9, 2022, Art. no. 2200175.

[61] Z. H. Guo, C. J. Gao, and H. Zhang, "Direction-dependent Janus metasurface supported by waveguide structure with spoof surface plasmon polariton modes," *Adv. Mater. Technol.*, vol. 8, no. 2, 2023, Art. no. 2200435.

[62] S. Guo, C. Hu, and H. Zhang, "Unidirectional ultrabroadband and wide-angle absorption in graphene-embedded photonic crystals with the cascading structure comprising the Octonacci sequence," *J. Opt. Soc. Amer. B*, vol. 37, no. 9, pp. 2678–2687, 2020.